Research Square

Preprints are preliminary reports that have not undergone peer review.
They should not be considered conclusive, used to inform clinical practice,
or referenced by the media as validated information.

Genome-scale metabolic reconstruction of *Cronobacter sakazakii* reveals essential metabolic pathways linked to pathogenicity and biofilm formation

Martin Muigano

muiganu@gmail.com

Bio One Scientific https://orcid.org/0000-0002-5986-1038

Research Article

Keywords: Cronobacter sakazakii, genome-scale metabolic model, biofilm, virulence, infant formula

Posted Date: September 11th, 2026

DOI: https://doi.org/10.21203/rs.3.rs-10989479/v1

License: This work is licensed under a Creative Commons Attribution 4.0 International License.
Read Full License

Additional Declarations: The authors declare no competing interests.

Abstract

Cronobacter sakazakii is an opportunistic foodborne pathogen associated with life-threatening infections in neonates fed with contaminated powdered infant formula. Here, I present iMN1443, a curated genome-scale metabolic model (GEM) for *C. sakazakii* ATCC BAA-894 for the purpose of understanding its metabolic versatility, biofilm persistence, or virulence-associated metabolism. The model was reconstructed from its annotated genome using CarveMe and iteratively refined through manual curation, gap-filling, and flux balance analysis (FBA). The final model comprises 2,902 reactions, 1,849 metabolites, and 1,443 genes (73.2% gene-protein-reaction coverage), a growth rate of 0.893 h^{-1} on glucose minimal medium, and a MEMOTE score of 93%. iMN1443 correctly reproduced utilization of fourteen carbon sources characteristic of dairy and infant-formula environments. When calibrated against empirical *Cronobacter* growth trajectories across two temperatures and two culture volumes, the GEM captured 91.8%–98.4% of the experimental variance. Flux analysis revealed a highly active, fully oxidative central carbon metabolism supporting substantial ATP synthase flux. Comparison of standard and parsimonious FBA highlighted extensive pathway redundancy. Simulating six host- and biofilm-associated microenvironments further revealed a pronounced growth-virulence trade-off: growth declined up to 14-fold from laboratory medium to the biofilm interior while the macrophage phagolysosome triggered a 308-fold upregulation of reactive oxygen species defense pathways alongside collapse of oxidative energy metabolism. Simulated biofilm depth stratification showed a similar growth decline (up to 88%) accompanied by maintained biofilm-associated pathway flux. This is consistent with a persister-like survival strategy in nutrient- and oxygen-depleted zones. Genome-wide single-gene deletion analysis identified 107 essential genes that are predominantly involved in amino acid, nucleotide, and cell-envelope biosynthesis. These represent candidate antimicrobial targets. iMN1443 provides a metabolic modeling framework for *C. sakazakii* and a foundation for rational antimicrobial target discovery and food-safety risk assessment.

Introduction

Cronobacter sakazakii is a common contaminant of powdered infant formula (PIF). It has been implicated in disease outbreaks associated with contaminated infant formula. This opportunistic pathogen is associated with life-threatening infections such as meningitis, enterocolitis, and sepsis in infants and neonates (Singh et al., 2015). In the United States, an incidence of > 9 infections per 100,000 neonates has been reported (Kalyantanda et al., 2015). With mortality rates estimated to be as high as 40–80%, *C. sakazakii* infections remain a major public health concern (Moumane et al., 2026). This Gram-negative bacterium was first described in 1980 as Enterobacter sakazakii and subsequently reclassified to the *Cronobacter* genus in 2007 (Iversen et al., 2007). *Cronobacter* species, including *Cronobacter sakazakii*, occur in the natural environment and have been isolated from animals, plants, foods and environmental sources (World Health Organization, 2025).

C. sakazakii has unique adaptations that allow its persistence in powdered infant formula. First, it has remarkable osmotolerance that aids its survival in dry powder (Lee et al., 2021). While desiccation is a

key osmotic stress, *C. sakazakii* cells are able to survive in such conditions. This could be attributed to the presence of osmoprotective biomolecules like trehalose (Feeney et al., 2015). Besides the unique osmotolerance, *C. sakazakii* benefits from its biofilm formation ability that further aids its survival (Ling et al., 2020). The bacterium achieves this through the formation of extracellular polysaccharide (EPS) for enhanced surface conditioning, cell adhesion, and formation of microcolonies (Henry & Fouladkhah, 2019). Additionally, this pathogen is able to utilize a broad range of nutrients. This broad nutrient utilization alongside its metabolic versatility allows the bacterium to survive in nutrient-limiting conditions. However, genome-scale metabolic modeling is yet to be applied for understanding the metabolism of *C. sakazakii*.

Genome-scale metabolic models (GEMs) constitute the mathematical summaries of reactions that are encoded by the genome of an organism. GEMs are the metabolic frameworks of all information of an organism such as genes, reactions, metabolites, enzyme, and gene-protein-reaction (GPR) rules (Passi et al., 2021). These models enable the simulation of metabolic phenotypes under diverse environmental conditions. They are also useful for prediction of growth rates across substrates, identification of essential genes and metabolic bottlenecks, and rational design of metabolic engineering strategies (Bernstein et al., 2021; Zhang & Hua, 2016). As such, GEMs are essential for understanding pathogen metabolism and biology. Previous successful applications in this area include *Mycobacterium tuberculosis*, *Pseudomonas aeruginosa*, and *Mycobacterium abscessus*. Despite *C. sakazakii*'s clinical importance, no comprehensive, publicly available GEM exists for this organism. This limits our predictive capability regarding its metabolic behavior under food-processing conditions. Here, I present iMN1443, a curated GEM for *C. sakazakii* BAA-894. The model was specifically designed to address three key biological questions: (1) What metabolic strategies enable *C. sakazakii* to survive biofilm formation across oxygen and nutrient gradients in food-processing environments? (2) Which genes and reactions are essential for growth, and which represent metabolic redundancy? (3) Which metabolic targets unique to *C. sakazakii* offer a safety window for antimicrobial development?

Materials and Methods

Strains and Data

Genome-scale metabolic reconstruction was based on *Cronobacter sakazakii* BAA-894. The annotated genome of this bacterium came from a previous publication (Kucerova et al., 2010) and was retrieved from the National Center for Biotechnology Information (NCBI) Genomes under the accession number GCF_000017665.1. The annotated genome had a size of 4.5 Mb with 3 chromosomes, 3 contigs, and a GC content of 56.5%. The strain was isolated from powdered milk formula fed to a hospitalized neonate. Growth data was obtained from a previous report (Parra-Flores et al., 2015).

Draft model reconstruction

The draft metabolic model for *C. sakazakii* BAA-894 was generated using CarveMe v1.5.1 from the annotated reference genome (RefSeq ID: GCF_000017665.1) obtained from the NCBI Genomes database. CarveMe employs a gap-free approach using universal core and organism-specific templates derived from the Model SEED database (Machado et al., 2018). The draft model was exported in Systems Biology Markup Language (SBML Level 3) format and imported into COBRApy (version 0.31.1) for manual inspection and refinement (Ebrahim et al., 2013). The initial draft model contained 2,847 reactions, 1,849 metabolites, and 1,443 genes organized across three cellular compartments (cytosol C_c, periplasm C_p, extracellular space C_e). Quality assessment was consistently evaluated with MEMOTE (Lieven et al., 2020).

Manual curation and gap filling

The curation process began with the refinement of genome annotations. The reconstructed metabolic model retained NCBI RefSeq protein accession numbers (WP_ identifiers) as gene identifiers. This ensured direct correspondence with the reference genome of *Cronobacter sakazakii* ATCC BAA-894 (RefSeq assembly GCF_000017665.1). However, to enhance annotation completeness and compliance with community standards, Systems Biology Ontology (SBO) terms were incorporated for all metabolites, reactions, and genes. The annotation structures inherited from the CarveMe universal template were standardized by converting list-based Python objects into dictionary-formatted annotations containing explicit identifier keys. These modifications improved interoperability with SBML-compliant software and enabled successful evaluation using the MEMOTE benchmarking framework. The final model had identifiers linked to RefSeq, NCBI Gene, UniProt, and KEGG Orthology identifiers. These annotations substantially improved gene–protein–reaction (GPR) associations and enabled subsequent analyses including reaction essentiality, gene essentiality, pathway enrichment, and virulence-associated metabolic investigations.

Model curation was then performed iteratively using COBRApy by combining flux balance analysis (FBA), reaction inspection, literature-supported biochemical knowledge, genome annotation, and pathway completeness analyses. First, the generated model from CarveMe produced several reactions that had stoichiometric inconsistency. For example, the β-galactosidase reaction was imbalanced due to the lack of a critical reactant. This reaction was manually corrected to align with established catalytic mechanism of β-galactosidase. Similar inconsistencies were inspected throughout the network using mass- and charge-balance diagnostics together with Memote quality assessment.

Growth simulations further revealed that central carbon metabolism contained several blocked reactions. Flux variability analysis and reaction inspection identified inappropriate reaction reversibility constraints within glycolysis that prevented normal carbon flow. The directionalities of phosphofructokinase (PFK) and pyruvate kinase (PYK), two irreversible rate-limiting glycolytic enzymes, were manually corrected to reflect physiological constraints. This restored complete glycolytic flux from glucose to pyruvate. Further model analysis revealed that intracellular pyruvate could not support growth because the reconstruction lacked a transport reaction connecting extracellular pyruvate with the

cytosol. To resolve this gap, a pyruvate transport reaction (PYRt) was introduced (pyr_e ⇌ pyr_c). This enabled the physiologically realistic utilization of pyruvate as a sole carbon source. Additional rounds of gap filling focused on amino acid biosynthesis. Initial simulations predicted several auxotrophies that are inconsistent with the known prototrophic nature of *Cronobacter sakazakii*. Missing reactions were identified and incorporated where genomic evidence supported their presence. Incorrect reaction constraints were adjusted where necessary. This process restored complete biosynthetic capability for essential amino acids and substantially improved biomass production under minimal medium conditions.

Additionally, reaction reversibility was evaluated by examining reaction stoichiometry, flux variability analysis (FVA), and known biochemical thermodynamics. Several reactions initially assigned reversible bounds (-1000 to 1000 mmol gDW^{-1} h^{-1}) were identified as physiologically irreversible. Specifically, the phosphofructokinase reaction (PFK) [ATP + fructose-6-phosphate → ADP + fructose-1,6-bisphosphate + H^+] was constrained to operate only in the forward direction by setting the lower bound to zero. Similarly, the pyruvate kinase reaction (PYK) [phosphoenolpyruvate + ADP + H^+ → pyruvate + ATP] was constrained to the forward direction (lower bound = 0). These modifications were implemented to prevent thermodynamically infeasible reverse fluxes while preserving model growth.

Model behavior was repeatedly evaluated after every curation step using flux balance analysis, flux variability analysis, and pathway connectivity analysis. To improve network quality, duplicate reactions, redundant transport reactions, blocked pathways, and thermodynamically infeasible flux cycles were systematically investigated. Duplicate biochemical reactions sharing identical stoichiometric equations were identified computationally and manually inspected to distinguish biologically meaningful isoenzymes from redundant reactions introduced during automated reconstruction. Candidate reactions were inspected individually and corrected where necessary. Following iterative curation, the final model exhibited stable aerobic growth on glucose minimal medium with a predicted biomass production rate of 0.893 h^{-1} while maintaining realistic ATP maintenance requirements.

Model Simulations

All simulations were conducted on a minimal medium. The minimal medium consisted of glucose as the sole carbon source (10 mmol gDW^{-1} h^{-1}), ammonium as the primary nitrogen source (10 mmol gDW^{-1} h^{-1}), sulfate (5 mmol gDW^{-1} h^{-1}), phosphate (10 mmol gDW^{-1} h^{-1}), and oxygen (20 mmol gDW^{-1} h^{-1}). Essential inorganic ions and trace elements, including K^+ (1 mmol gDW^{-1} h^{-1}), Na^+ (1 mmol gDW^{-1} h^{-1}), Ca^{2+} (0.1 mmol gDW^{-1} h^{-1}), Cl^- (0.2 mmol gDW^{-1} h^{-1}), Mg^{2+} (0.2 mmol gDW^{-1} h^{-1}), Fe^{2+} (1 mmol gDW^{-1} h^{-1}), Zn^{2+} (0.01 mmol gDW^{-1} h^{-1}), Mn^{2+} (0.01 mmol gDW^{-1} h^{-1}), Co^{2+} (0.01 mmol gDW^{-1} h^{-1}), Cu^{2+} (0.01 mmol gDW^{-1} h^{-1}), and molybdate (0.01 mmol gDW^{-1} h^{-1}) were supplied at the specified uptake rates. Water and protons were supplied at non-limiting uptake rates (1000 mmol gDW^{-1} h^{-1}). All other organic compounds, amino acids, vitamins, and alternative carbon sources were excluded from the medium unless otherwise specified for a particular simulation.

Constraint-based simulations were performed using the COBRApy package (version 0.31.1) implemented in Python. The curated genome-scale metabolic model was analyzed under the assumption of a pseudo-steady state whereby intracellular metabolite concentrations remain constant over time. Further, it was assumed that the net production and consumption of each metabolite satisfy the mass-balance constraint: $Sv = 0$, where S represents the stoichiometric matrix and v is the vector of reaction fluxes constrained by reaction-specific lower and upper bounds. Unless otherwise stated, the biomass synthesis reaction was defined as the objective function and optimized using flux balance analysis (FBA) (Orth et al., 2010). The ATP maintenance reaction (ATPM) was constrained to the calibrated value of 8.39 mmol gDW^{-1} h^{-1} to reproduce physiologically realistic growth. All simulations were performed under an aerobic minimal medium. Glucose uptake was constrained to − 10 mmol gDW^{-1} h^{-1} and oxygen uptake to − 20 mmol gDW^{-1} h^{-1}. The medium allowed exchange reactions for ammonium, phosphate, sulfate, water, protons and essential inorganic ions. Under these conditions, the optimized biomass objective function corresponded to the predicted specific growth rate (h^{-1}), since the model was normalized to 1 g dry cell weight.

The metabolic capabilities of the model were evaluated through a series of *in silico* simulations. Carbon source utilization was assessed by replacing glucose with individual substrates while maintaining all other medium components unchanged, and growth was evaluated from the resulting biomass flux. Flux variability analysis (FVA) was subsequently performed to determine the minimum and maximum allowable flux through each reaction while maintaining 100% of the optimal growth rate. This made it possible to identify reactions with constrained or flexible metabolic behavior. To further characterize the feasible solution space, flux sampling was performed using the Artificial Centering Hit-and-Run (ACHR) algorithm implemented in COBRApy, and reaction flux distributions were summarized using descriptive statistics and principal component analysis.

Model calibration and benchmarking

To validate the predictive accuracy and biological fidelity of the reconstructed genome-scale metabolic model iMN1443, a dynamic Flux Balance Analysis (dFBA) simulation framework was implemented. The computational model was benchmarked against digitized growth trajectory time-course data (0 to 24 h) from a published study evaluating *Cronobacter* growth mechanics in reconstituted powdered infant formula (Parra-Flores et al., 2015). The environmental constraints for the dFBA loop were configured to replicate the physical culture profiles of the study namely two incubation temperatures (22°C and 35°C) cross-evaluated across two vessel capacities (100 mL and 3000 mL). To account for temperature-dependent enzyme kinetics, substrate uptake dynamics were dynamically scaled using the Ratkowsky square-root biological temperature model:

$$T_{factor} = \left(\frac{T - T_{min}}{T_{opt} - T_{min}} \right)^2$$

Where T represents the cultivation temperature, T_{min} is the cardinal minimum growth temperature (3.5°C), T_{opt} is the optimal temperature (37°C), T_{factor} is the scaling factor. As highlighted previously, vessel-specific scaling was captured via oxygen mass transfer limitations with 20 mmol. $gDCW^{-1}.h^{-1}$ for 100 mL and 12 mmol. $gDCW^{-1}.h^{-1}$ for 3000 mL. Additionally micro-minerals and essential housekeeping ions were incorporated in the simulation medium. Baseline bacteria population was set at 1.71 $\log_{10}$ CFU/mL to mirror the starting titers in the published study while factoring the empirical lag phases (λ) unique to each profile. To capture the transition from exponential growth to the stationary phase plateau (N_{max}), an automated high-order logistic deceleration scaling factor (SF) was integrated into the continuous integration step:

$$SF = 1.0 - \left(\frac{N_t}{N_{max}} \right)^4$$

$$\mu_{eff} = \mu_{eff} . \max(0, SF)$$

where N_t is the population density at time t, N_{max} is the carrying capacity, and μ_{eff} is the biologically adjusted specific growth rate used to compute cellular accumulation at a step size of dt = 0.1 h. The mathematical predictive capacity of iMN1443 was rigorously evaluated by measuring the coefficient of determination (R2) to determine the proportion of experimental variance explained by the metabolic model:

$$R^2 = 1 - \frac{\sum_{i=1}^{n} \left(y_i - \hat{\mathrm{y}}_i \right)^2}{\sum_{i=1}^{n} \left(y_i - \bar{y}_i \right)^2}$$

where y_i represents the digitized empirical data points extracted from the literature, $\hat{\mathrm{y}}_i$ denotes the linearly interpolated dFBA model predictions at the identical time coordinates, and $\bar{y}_i$ represents the arithmetic mean of the empirical literature dataset.

Biofilm Analysis

To model pathogen metabolism in distinct host microenvironments, I modified nutrient uptake rates in the GEM to reflect physiologically accurate concentrations. Laboratory medium served as the control with unrestricted nutrient availability (glucose 10 mM, oxygen 20 mM, iron 1000 μM). Intestinal epithelium conditions approximated microaerobic biofilm-like environments (glucose 8 mM, oxygen 5 mM, iron 1000 μM), while blood/serum conditions reflected systemic infection with limited glucose and severe iron sequestration (glucose 5 mM, oxygen 15 mM, iron 0.01 μM). Macrophage phagolysosome conditions represented the most hostile environment, with combined nutrient limitation and metabolic stress (glucose 2 mM, oxygen 0.5 mM, iron 0.1 μM, pH 4.8). Cerebrospinal fluid conditions modeled meningitis-associated constraints (glucose 2.5 mM, oxygen 10 mM, iron 0.001 μM). Critically, biofilm interior conditions incorporated nitrate as an alternative electron acceptor (nitrate 5 mM, oxygen 0.2 mM, glucose 2.0 mM), enabling anaerobic respiration and persister cell viability. All environmental

simulations maintained basal requirements for ATP (8.39 mmol/gDCW/h) and nucleotide biosynthesis (0.5 mmol/gDCW/h) to reflect metabolically competent but growth-limited cell states.

Results and Discussion

Genome-scale metabolic model reconstruction

The genome scale metabolic model of *Cronobacter sakazakii* ATCC BAA-894 (iMN1443) comprised 2,902 reactions, 1,849 metabolites, and 1,443 genes. The model had three cellular compartments namely the cytosol (C_c), periplasm (C_p), and extracellular space (C_e). Flux balance analysis (FBA) predicted a biomass growth rate of 0.689 h^{-1} on the default medium. The model contained 2,426 internal reactions, 414 exchange reactions, 53 demand reactions, and 8 sink reactions. This shows that the model had extensive metabolic coverage of central metabolism, transport processes, and biomass biosynthesis pathways. Gene-protein-reaction (GPR) associations were assigned to 2,124 reactions, corresponding to a GPR coverage of 73.2%. Hence, the majority of metabolic functions were supported by genomic evidence. The reconstructed network captured key pathways involved in carbohydrate metabolism, amino acid biosynthesis, energy generation, and nutrient transport.

The model was then tested for growth on various substrates. As shown in Table 1, among the tested substrates, glucose, galactose, and lactose supported the highest biomass production (0.893 h^{-1}) on minimal media. Thus, the bacterium has efficient utilization of sugars commonly encountered in dairy and infant formula environments. Growth was also supported by gluconate-derived substrates, including gluconate (0.868 h^{-1}), glucuronate (0.788 h^{-1}), and 2-dehydrogluconate (0.887 h^{-1}). Organic acids such as citrate (0.747 h^{-1}), succinate (0.580 h^{-1}), acetate (0.352 h^{-1}), and pyruvate (0.530 h^{-1}) supported lower but substantial growth rates. Amino acids including glutamate, aspartate, and alanine also served as effective carbon and energy sources. Therefore, *C. sakazakii* has a strong metabolic versatility. This extensive substrate utilization profile demonstrates that the model was capable of reproducing the broad nutritional flexibility characteristic of opportunistic Enterobacteriaceae.

Table 1
Predicted growth rates of iMN1443 on selected carbon sources under aerobic minimal medium conditions.

Carbon source	Exchange reaction	Predicted growth rate (h^{-1})
Glucose	EX_glc__D_e	0.893
Galactose	EX_gal_e	0.893
Lactose	EX_lcts_e	0.893
2-Dehydrogluconate	EX_2dhglcn_e	0.887
Gluconate	EX_glcn_e	0.868
Glucuronate	EX_glcur_e	0.788
Citrate	EX_cit_e	0.747
Glutamate	EX_glu__L_e	0.712
Glycerol	EX_glyc_e	0.659
Aspartate	EX_asp__L_e	0.599
Succinate	EX_succ_e	0.580
Alanine	EX_ala__L_e	0.548
Pyruvate	EX_pyr_e	0.530
Acetate	EX_ac_e	0.352

Analysis of Flux Distribution

Opportunistic pathogens like *Cronobacter sakazakii* are known for their metabolic adaptability. This helps them to thrive in diverse environments and to coordinate complex cellular functions. However, the precise characterization of these pathways remains challenging because of the reliance on traditional, trial-and-error experimental methodologies. Using the iMN1443 model, I performed flux balance analysis under glucose minimal medium conditions. Figure 1 shows the systems-level view of the metabolic organization of *C. sakazakii*. As earlier indicated, the model achieved a growth rate of 0.893 h^{-1} on minimal medium. Glucose uptake was constrained to 10 mmol gDW^{-1} h^{-1}, with carbon entering central metabolism through the phosphoenolpyruvate:sugar phosphotransferase system (GLCpts). GLCpts then generated intracellular glucose-6-phosphate and pyruvate. The principal carbon flux subsequently proceeded through the Embden–Meyerhof–Parnas (EMP) pathway with glucose-6-phosphate isomerase (PGI) carrying 9.26 mmol gDW^{-1} h^{-1}, followed by phosphofructokinase (PFK) and fructose-bisphosphate aldolase (FBA), each carrying 8.83 mmol gDW^{-1} h^{-1}. Glyceraldehyde-3-phosphate dehydrogenase (GAPD) carried a higher flux of 16.62 mmol gDW^{-1} h^{-1}. This points to the conversion of the two three-carbon intermediates generated by the aldolase reaction. Downstream reactions included phosphoglycerate

kinase (16.62 mmol gDW^{-1} h^{-1}), phosphoglycerate mutase (15.65 mmol gDW^{-1} h^{-1}), and enolase (15.65 mmol gDW^{-1} h^{-1}).

Pyruvate represented a major metabolic branch point whereby the dominant oxidative route proceeding through pyruvate dehydrogenase (PDH) at 7.74 mmol gDW^{-1} h^{-1}. This generated acetyl-CoA for entry into the tricarboxylic acid (TCA) cycle. In contrast, pyruvate formate lyase (PFL; 0.096 mmol gDW^{-1} h^{-1}) and pyruvate:ferredoxin oxidoreductase (PFOR; 0.095 mmol gDW^{-1} h^{-1}) contributed only minor fluxes. Acetyl-CoA subsequently entered the TCA cycle through citrate synthase (CS), followed by aconitase and isocitrate dehydrogenase (ICDHyr), with each carrying 7.35 mmol gDW^{-1} h^{-1}. Flux then continued through 2-oxoglutarate dehydrogenase (6.33 mmol gDW^{-1} h^{-1}) and succinate dehydrogenase (6.33 mmol gDW^{-1} h^{-1}). The model also predicted substantial anaplerotic activity through phosphoenolpyruvate carboxylase (2.77 mmol gDW^{-1} h^{-1}). This likely shows that carbon flux was not restricted exclusively to oxidative metabolism but was also directed toward replenishment of biosynthetic intermediates. The energetic requirements of this highly aerobic metabolic state were supported by strong respiratory-chain comprising NADH dehydrogenase (NADH16pp) (33.37 mmol gDW^{-1} h^{-1}) and cytochrome bo_3 oxidase (CYTBO3_4pp) (40.00 mmol gDW^{-1} h^{-1}). Proton translocation through the respiratory chain supported ATP synthase (ATPS4rpp), which carried 56.89 mmol gDW^{-1} h^{-1}. Overall, the flux distribution predicted by iMN1443 indicates that aerobic growth on glucose is dominated by glycolytic carbon processing, oxidative conversion of pyruvate through PDH, active TCA-cycle metabolism, and strong respiratory phosphorylation.

To evaluate the metabolic flux distribution of the *Cronobacter sakazakii* model (iMN1443), I compared standard Flux Balance Analysis (FBA) with parsimonious Flux Balance Analysis (pFBA). The results are summarized in Fig. 2. While standard FBA maximizes the objective function, and parsimonious FBA minimizes total cellular flux while maintaining optimal growth. The analysis revealed a growth rate of 0.893 h^{-1}. for both FBA and pFBA. However, pFBA achieved this with a significantly lower total flux (608.53 vs. 668.23) and fewer active reactions (302 vs. 310). This reduction highlights the metabolic redundancy present in the model. It means that the cell can optimize its resources by minimizing unnecessary flux through parallel pathways. Now, looking at the flux distribution, it was evident that the highest fluxes in both models are associated with ATP synthesis, water demand, and respiratory chain components. The top flux carrying reactions are ATP synthase (ATPS4rpp), NADH dehydrogenase (NADH16pp) and Cytochrome oxidase bo3 (CYTBO3_4pp). When switching to pFBA, Cytochrome oxidase bd (CYTBDpp) displayed a major shift. Initially, it carried a flux of 10.12 mmol gDW^{-1} h^{-1} in FBA but it was completely inactive (0 flux) in the pFBA solution. This indicates that while CYTBDpp is capable of contributing to respiration, it is metabolically inefficient compared to the bo3 oxidase under the simulated conditions. Thus, the findings show that CYTBDpp is a non-parsimonious pathway. On the other hand, central metabolic pathways like glycolysis (GAPD, PGK, ENO, PGM) show flux reductions ranging from 8% to 13.5%. This shows that pFBA re-routes carbon flow to favor more efficient utilization. On the extreme end, transporters such as CO2tpp and O2tpp, and water demand (DM_h2o_c) show marginal changes in flux (0%–3%). This points to their essential role in maintaining homeostasis.

Virulence-Associated Metabolic Adaptation

Cronobacter sakazakii demonstrated environment-dependent metabolic phenotypes reflecting a growth-virulence trade-off hierarchy (Fig. 3). Maximum growth occurred in laboratory medium (0.893 h^{-1}). It then declined progressively across host niches: intestinal epithelium (0.298 h^{-1}), blood/serum (0.179 h^{-1}), macrophage phagolysosome (0.156 h^{-1}), cerebrospinal fluid (0.089 h^{-1}), and biofilm interior (0.064 h^{-1}). This 14-fold reduction in growth rate from permissive to biofilm conditions demonstrates severe metabolic constraints under in vivo conditions. Pathway-level analysis revealed dramatic metabolic reprogramming in the macrophage phagolysosome, the most hostile niche tested. Reactive oxygen species (ROS) defense pathways showed a 308-fold upregulation. This is consistent with the intense oxidative stress within this compartment. Conversely, central carbon metabolism was severely downregulated: TCA cycle flux decreased 19-fold, energy production flux declined 50-fold, and pentose phosphate pathway flux diminished 74-fold. It was also evident that glycolysis flux actually increased 1.1-fold in the macrophage despite overall growth reduction. This could be indicative of a shift toward fermentative metabolism to compensate for impaired oxidative phosphorylation.

Biofilm interior conditions permitted slow growth (0.064 h^{-1}) following introduction of nitrate as an alternative electron acceptor. This could be a pointer to the possibility that anaerobic respiration via denitrification sustains persister cell metabolism in biofilm cores. Biofilm-associated pathway flux remained relatively high (52 mmol/gDCW/h in macrophage vs. 59 in lab), representing 88% of laboratory levels despite 17-fold growth reduction. Hence, it is likely that *C. sakazakii* maintains biofilm factor synthesis even under severe metabolic stress. Thus, this is probably a critical virulence trait enabling persistent infection.

Gene Essentiality Analysis

To identify genes required for growth and survival, a genome-wide in silico single-gene deletion analysis was performed using the curated *Cronobacter sakazakii* metabolic model iMN1443. The wild-type model achieved a predicted growth rate of 0.8931 h^{-1} under the defined minimal medium conditions. Each of the 1,443 genes in the model was individually deleted and the resulting growth phenotype evaluated using flux balance analysis. The gene essentiality analysis revealed that the majority of genes were non-essential under the simulated growth conditions. Of the 1,443 genes evaluated, 1,312 genes (90.9%) were classified as non-essential, while deletion of 107 genes (7.4%) completely abolished growth and these were therefore classified as essential. An additional 23 genes (1.6%) resulted in a reduced-growth phenotype. These are the genes that contribute to metabolic fitness but are not strictly required for biomass formation. Functional annotation of the predicted essential genes using UniProt identified several biological processes that were disproportionately enriched among lethal gene knockouts (Fig. 4). Amino acid biosynthesis constituted the largest category, accounting for 31 essential genes. This highlights the central role of anabolic pathways in sustaining biomass production and cellular growth. Essential genes were also highly represented in core metabolic processes (12 genes) and purine biosynthesis (10 genes). This is testament to the critical importance of energy generation, precursor

metabolite production, and nucleotide synthesis. Several additional cellular functions contained substantial numbers of essential genes, including histidine biosynthesis, aromatic amino acid biosynthesis, cell wall biogenesis/degradation, cell shape determination, peptidoglycan synthesis, cell cycle regulation, and cell division. These processes are linked to cellular integrity, replication, and maintenance of bacterial morphology. Smaller groups of essential genes were associated with branched-chain amino acid biosynthesis, lysine biosynthesis, isoprenoid biosynthesis, menaquinone biosynthesis, and pyrimidine biosynthesis (Fig. 4). The predominance of essential genes involved in amino acid, nucleotide, and cell envelope biosynthesis suggests that these pathways represent major metabolic bottlenecks in *C. sakazakii*. These genes also represent the drug targets for this bacterium.

Metabolic heterogeneity across simulated biofilm zones

To investigate the metabolic adaptations of *Cronobacter sakazakii* within structured biofilms, the iMN1443 model was used to simulate four biofilm zones. These zones were designed to represent progressive gradients in oxygen and nutrient availability. The outer biofilm layer (0–100 μm) was modelled under aerobic, nutrient-rich conditions. Deeper layers were subjected to decreasing oxygen, glucose, and lactose concentrations. This culminated in an anaerobic, nutrient-depleted stationary zone (> 500 μm). The simulations predicted a pronounced decline in biomass production with increasing biofilm depth (Fig. 5). The outer aerobic zone exhibited the highest growth rate (0.689 h^{-1}) whereas growth decreased to 0.393 h^{-1} in the intermediate microaerophilic zone, 0.165 h^{-1} in the anaerobic core, and 0.083 h^{-1} in the stationary region. Relative to the biofilm surface, growth was reduced by 43%, 76%, and 88% in Zones 2, 3, and 4, respectively. A similar trend was observed for ATP generation. ATP production decreased sharply from 31.61 mmol $gDCW^{-1}$ h^{-1} in the outer aerobic region to 4.54 mmol $gDCW^{-1}$ h^{-1} in the intermediate zone. In the anaerobic and stationary zones, ATP synthase-associated flux approached zero. This points to severe energetic limitations under oxygen-depleted conditions. These findings suggest that biofilm formation in *C. sakazakii* is not a uniform multicellular structure. Instead, it constitutes a metabolically specialized community where the outer zone prioritizes growth and matrix synthesis while inner zones prioritize long-term survival.

Model calibration

The genome-scale metabolic model iMN1443 demonstrated high fidelity in capturing the dynamic, time-dependent growth kinetics of *Cronobacter* across varying thermal and volumetric scales. When evaluated against empirical literature data, the dFBA simulations reproduced the characteristic growth kinetics. The simulations reproduced the distinctive sigmoidal growth trajectories and stationary plateaus across all four evaluated culture environments. At sub-optimal ambient temperature (22°C), the model showed strong alignment with the published data, explaining 94.84% (R^2 = 0.948) of the variance for a 100 mL vessel ($\mu_{sim} = 1.08\ h^{-1}$). Under a scale-up condition (3,000 mL vessel), the model could predict 98.41% (R^2 = 0.984) of the experimental data. At the optimum temperature of 35°C, the metabolic infrastructure of iMN1443 maintained an equally strong predictive capability. The model

explained 92.48% (R^2= 0.925) of the growth variance in the 100 mL system. In the large-scale 3000 mL batch setup, the model accounted for 91.81% of the experimental variance (R^2= 0.918). This consistent alignment across these divergent physical constraints demonstrates that the metabolic network configuration within iMN1443 accurately routes internal flux behaviors. Hence, it may be a reliable in silico platform for simulating lifestyle dynamics in dietary matrix environments.

Discussion

Cronobacter sakazakii is a rare food pathogen that survives in dry foods like powdered infant formula. Despite its clinical and food-safety relevance, no comprehensive GEM exists for interrogating its metabolism in a quantitative, mechanistic framework. So, this study presents iMN1443, a curated genome-scale metabolic model of *Cronobacter sakazakii*. The model was reconstructed using an automated carving with CarveMe followed by iterative manual curation. The model's central carbon flux distribution predicted under glucose minimal medium was consistent with a highly oxidative Enterobacteriaceae lifestyle. This included a complete glycolytic transit, a fully closed TCA cycle, and substantial flux through NADH dehydrogenase, cytochrome bo_3 oxidase, and ATP synthase.

To understand the bacterium's virulence, host-niche simulations were conducted. They revealed a clear growth-virulence trade-off, with growth rate declining up to 14-fold between permissive laboratory medium and the most hostile simulated environments. An interesting feature of this trade-off was the 308-fold upregulation of reactive oxygen species defense pathways within the simulated macrophage phagolysosome. This occurred alongside a collapse in oxidative energy metabolism. This is consistent with the well-established role of the phagocyte NADPH oxidase (NOX2) complex in generating a bactericidal oxidative burst inside the phagosome (Bedard & Krause, 2007; Nauseef, 2019; Ţocu et al., 2025). Still, growth occurred in simulated macrophage phagolysosome at a rate of 0.156 h^{-1}. This is consistent with past evidence that *C. sakazakii* can survive and even multiply within macrophages and microglial cells rather than being cleared by them (Almajed & Forsythe, 2016; Townsend et al., 2007). The investment in oxidative stress defense at the expense of oxidative phosphorylation offers a plausible mechanistic explanation of intracellular survival. Experimental evidence has shown that *C. sakazakii* survives in macrophages environment by being able to resist oxidative stress (Liu et al., 2024). It is consistent with the nature of *C. sakazakii* as a pathogen equipped with multiple stress-survival systems that support both extra-intestinal persistence and desiccation tolerance in powdered formula (Feeney & Sleator, 2015).

To further understand the virulence features of *C. sakazakii*, biofilm zonation simulations were conducted. Specifically, a spatial dimension was added to the growth-virulence trade-off. Growth and ATP production declined progressively from the outer aerobic layer to the anaerobic, nutrient-depleted core. Viability in the deepest zones was only sustained once nitrate was introduced as an alternative electron acceptor. This mirrors a well-documented phenomenon in another Gram-negative biofilm-forming pathogen *Pseudomonas aeruginosa*. In *P. aeruginosa*, biofilms in the cystic fibrosis airway develop steep oxygen gradients (Worlitzsch et al., 2002). As a result, they become anaerobic in their

interior and rely on nitrate-dependent denitrification to sustain viable, respiring subpopulations deep within the biofilm matrix (Worlitzsch et al., 2002; Werner et al., 2004). The present simulations suggest that an analogous strategy may operate in *C. sakazakii* biofilms. A nitrate-dependent survival mechanism is therefore postulated for this organism. However, it is important to recognize that this hypothesis id based on computational grounds rather than experimental evidence. It was also observed that biofilm-associated pathway flux was maintained at a disproportionately high level (88% of laboratory levels) relative to the severe reduction in growth rate. This could suggest that matrix and adhesin synthesis is prioritized over biomass accumulation once cells enter this low-growth, stress-adapted state. This is important given that biofilm formation on feeding-tube and processing-equipment surfaces is a recognized route of powdered infant formula contamination (Henry & Fouladkhah, 2019).

Gene essentiality revealed a group of 107 essential genes in *C. sakazakii*. These essential genes were concentrated in amino acid biosynthesis, purine and pyrimidine biosynthesis, and cell envelope-related processes like peptidoglycan synthesis and cell division. Some of these genes, particularly those of peptidoglycan synthesis, represent pathways that are absent from human metabolism. Others like amino acid biosynthesis are supplied through diet rather than de novo biosynthesis. As such, these are attractive candidates for selective antimicrobial development. This is essential because multidrug-resistant *C. sakazakii* isolates have already reported from both clinical infections and contaminated infant food and food-processing environments (Gan et al., 2022). These isolates have been reported to carry acquired resistance to beta-lactams, tetracyclines, and other antimicrobial classes. As such, there is need for new target classes rather than reliance on existing antibiotics alone.

Several limitations of this work should be acknowledged. First, standard FBA assumes a pseudo-steady state. This means that it does not incorporate thermodynamic directionality or transcriptional and post-translational regulation. This means that reported fluxes might represent the metabolic capacity of the network rather than a guaranteed physiological outcome. Second, the predictions of this model are limited to the current curation efforts. As previously noted, gene-protein-reaction associations were available for only 73.2% of reactions. So, a substantial fraction of the model was gap-filled without direct genomic support and should be treated as provisional pending further annotation. Third, the biofilm zones and host-niche microenvironments were implemented as discrete, literature-parameterized nutrient and oxygen constraints rather than as an emergent outcome of a spatially resolved reaction-diffusion model. Therefore, the exact flux magnitudes should not be over-interpreted. Fourth, iMN1443 is based on a single reference strain (BAA-894) and may not fully capture the metabolic diversity reported across *Cronobacter* species and clinical isolates. Lastly, the essential gene predictions reported here are in silico and require experimental confirmation. Thus, future studies should address these limitations. Specifically, future studies may incorporate transcriptomic or proteomic data. Also, expanding the reconstruction to a pan-genome or multi-strain framework would clarify how much of the predicted metabolic behavior generalizes across the *Cronobacter* genus.

Conclusion

This study presents iMN1443, a curated genome-scale metabolic model of *Cronobacter sakazakii*. The model demonstrates its utility across three complementary lines of inquiry. First, the model accurately reproduced experimentally observed growth kinetics across multiple temperatures and culture volumes while capturing physiologically realistic range of carbon source utilization. Second, simulations of host-associated and biofilm microenvironments revealed a consistent growth-virulence trade-off. This trade-off is characterized by dramatic reprogramming of oxidative stress defense and central carbon metabolism under macrophage-like conditions and nitrate-dependent anaerobic persistence within simulated biofilm cores. Third, genome-wide gene essentiality analysis identified 107 genes that are concentrated in amino acid, nucleotide, and cell-envelope biosynthesis. These represent plausible antimicrobial targets with a potential safety window relative to human metabolism. Together, these findings position iMN1443 as a viable platform for investigating *C. sakazakii* metabolism, biofilm persistence, and host adaptation. Beyond the specific predictions reported here, this reconstruction provides a foundation for future systems-level studies. These include multi-omics integration, pan-genome expansion across *Cronobacter* species, and experimentally guided antimicrobial target prioritization. Such efforts are pathways to effective clinical management of neonatal infections and food-safety risk mitigation in powdered infant formula production.

Declarations

Data Availability

The genome-scale metabolic model generated in this study (iMN1443, SBML Level 3 format) is publicly available at https://github.com/ngangao/Cronobacter-GSMM1. Analysis and curation scripts are available from the corresponding author upon reasonable request.

References

1. Almajed FS, Forsythe SJ (2016) *Cronobacter sakazakii* clinical isolates overcome host barriers and evade the immune response. Microb Pathog 90:55–63. https://doi.org/10.1016/j.micpath.2015.11.014
2. Bedard K, Krause K-H (2007) The NOX Family of ROS-Generating NADPH Oxidases: Physiology and Pathophysiology. Physiol Rev 87(1):245–313. https://doi.org/10.1152/physrev.00044.2005
3. Bernstein DB, Sulheim S, Almaas E, Segrè D (2021) Addressing uncertainty in genome-scale metabolic model reconstruction and analysis. Genome Biol 22(1):64. https://doi.org/10.1186/s13059-021-02289-z
4. Ebrahim A, Lerman JA, Palsson BO, Hyduke DR (2013) COBRApy: COnstraints-Based Reconstruction and Analysis for Python. BMC Syst Biol 7(1):74. https://doi.org/10.1186/1752-0509-7-74
5. Feeney A, Kropp KA, O'Connor R, Sleator RD (2015) *Cronobacter sakazakii*: Stress survival and virulence potential in an opportunistic foodborne pathogen. Gut Microbes 5(6):711–718. https://doi.org/10.4161/19490976.2014.983774

6. Feeney A, Sleator RD (2015) Functional Screening of the *Cronobacter sakazakii* BAA-894 Genome reveals a role for ProP (ESA_02131) in carnitine uptake. Bioengineered 6(3):161–165. https://doi.org/10.1080/21655979.2015.1043500
7. Gan X, Li M, Xu J, Yan S, Wang W, Li F (2022) Emerging of Multidrug-Resistant *Cronobacter sakazakii* Isolated from Infant Supplementary Food in China. Microbiol Spectr 10(5):e01197–e01122. https://doi.org/10.1128/spectrum.01197-22
8. Henry M, Fouladkhah A (2019) Outbreak History, Biofilm Formation, and Preventive Measures for Control of *Cronobacter sakazakii* in Infant Formula and Infant Care Settings. Microorganisms 7(3):77. https://doi.org/10.3390/microorganisms7030077
9. Iversen C, Lehner A, Mullane N, Bidlas E, Cleenwerck I, Marugg J, Fanning S, Stephan R, Joosten H (2007) The taxonomy of Enterobacter sakazakii: Proposal of a new genus *Cronobacter* gen. nov. and descriptions of *Cronobacter sakazakii* comb. nov. *Cronobacter sakazakii* subsp. sakazakii, comb. nov., *Cronobacter sakazakii* subsp. malonaticus subsp. nov., *Cronobacter* turicensis sp. nov., *Cronobacter* muytjensii sp. nov., *Cronobacter* dublinensis sp. nov. and *Cronobacter* genomospecies 1. BMC Evol Biol 7(1):64. https://doi.org/10.1186/1471-2148-7-64
10. Kalyantanda G, Shumyak L, Archibald LK (2015) *Cronobacter* Species Contamination of Powdered Infant Formula and the Implications for Neonatal Health. Front Pead 3:56. https://doi.org/10.3389/fped.2015.00056
11. Kucerova E, Clifton SW, Xia X-Q, Long F, Porwollik S, Fulton L, Fronick C, Minx P, Kyung K, Warren W, Fulton R, Feng D, Wollam A, Shah N, Bhonagiri V, Nash WE, Hallsworth-Pepin K, Wilson RK, McClelland M, Forsythe SJ (2010) Genome Sequence of *Cronobacter sakazakii* BAA-894 and Comparative Genomic Hybridization Analysis with Other *Cronobacter* Species. PLoS ONE 5(3):e9556. https://doi.org/10.1371/journal.pone.0009556
12. Lee K, Koyama K, Kawai K, Koseki S (2021) Why Does *Cronobacter sakazakii* Survive for a Long Time in Dry Environments? Contribution of the Glass Transition of Dried Bacterial Cells. Microbiol Spectr 9(3):e01384–e01321. https://doi.org/10.1128/spectrum.01384-21
13. Lieven C, Beber ME, Olivier BG, Bergmann FT, Ataman M, Babaei P, Bartell JA, Blank LM, Chauhan S, Correia K, Diener C, Dräger A, Ebert BE, Edirisinghe JN, Faria JP, Feist AM, Fengos G, Fleming RMT, García-Jiménez B, Zhang C (2020) MEMOTE for standardized genome-scale metabolic model testing. Nat Biotechnol 38(3):272–276. https://doi.org/10.1038/s41587-020-0446-y
14. Ling N, Forsythe S, Wu Q, Ding Y, Zhang J, Zeng H (2020) Insights into *Cronobacter sakazakii* Biofilm Formation and Control Strategies in the Food Industry. Engineering 6(4):393–405. https://doi.org/10.1016/j.eng.2020.02.007
15. Liu Y, Zhang J, Zhao H, Zhong F, Li J, Zhao L (2024) VBNC *Cronobacter sakazakii* survives in macrophages by resisting oxidative stress and evading recognition by macrophages. BMC Microbiol 24(1):458. https://doi.org/10.1186/s12866-024-03595-9
16. Machado D, Andrejev S, Tramontano M, Patil KR (2018) Fast automated reconstruction of genome-scale metabolic models for microbial species and communities. Nucleic Acids Res 46(15):7542–

7553. https://doi.org/10.1093/nar/gky537

17. Moumane O, Gómez-Llorente H, Barat JM, Pérez-Esteve É, Rivas A (2026) Mitigating *Cronobacter sakazakii* safety risks associated with non-uniform reconstitution of infant formula using silica-immobilized phenolic compounds. Innovative Food Science Emerging Technologies 109:104484. https://doi.org/10.1016/j.ifset.2026.104484
18. Nauseef WM (2019) The phagocyte NOX2 NADPH oxidase in microbial killing and cell signaling. Curr Opin Immunol 60:130–140. https://doi.org/10.1016/j.coi.2019.05.006
19. Orth JD, Thiele I, Palsson BØ (2010) What is flux balance analysis? Nat Biotechnol 28(3):245–248. https://doi.org/10.1038/nbt.1614
20. Parra-Flores J, Rodriguez A, Riffo F, Arvizu-Medrano SM, Arias-Rios EV, Aguirre J (2015) Investigation on the Factors Affecting *Cronobacter sakazakii* Contamination Levels in Reconstituted Powdered Infant Formula. Front Pead 3:72. https://doi.org/10.3389/fped.2015.00072
21. Passi A, Tibocha-Bonilla JD, Kumar M, Tec-Campos D, Zengler K, Zuniga C (2021) Genome-Scale Metabolic Modeling Enables In-Depth Understanding of Big Data. Metabolites 12(1):14. https://doi.org/10.3390/metabo12010014
22. Singh N, Goel G, Raghav M (2015) Insights into virulence factors determining the pathogenicity of *Cronobacter sakazakii*. Virulence 6(5):433–440. https://doi.org/10.1080/21505594.2015.1036217
23. Țocu G, Ștefănescu BI, Stavăr Matei L, Țocu L (2025) Phagocyte NADPH Oxidase NOX2-Derived Reactive Oxygen Species in Antimicrobial Defense: Mechanisms, Regulation, and Therapeutic Potential—A. Narrative Rev Antioxidants 15(1):55. https://doi.org/10.3390/antiox15010055
24. Townsend SM, Hurrell E, Gonzalez-Gomez I, Lowe J, Frye JG, Forsythe S, Badger JL (2007) Enterobacter sakazakii invades brain capillary endothelial cells, persists in human macrophages influencing cytokine secretion and induces severe brain pathology in the neonatal rat. Microbiology 153(10):3538–3547. https://doi.org/10.1099/mic.0.2007/009316-0
25. World Health Organization (2025) Cronobacter sakazakii: Background document for the WHO guidelines for drinking-water quality. World Health Organization. https://doi.org/10.2471/B09255
26. Worlitzsch D, Tarran R, Ulrich M, Schwab U, Cekici A, Meyer KC, Birrer P, Bellon G, Berger J, Weiss T, Botzenhart K, Yankaskas JR, Randell S, Boucher RC, Döring G (2002) Effects of reduced mucus oxygen concentration in airway Pseudomonas infections of cystic fibrosis patients. J Clin Invest 109(3):317–325. https://doi.org/10.1172/JCI0213870
27. Zhang C, Hua Q (2016) Applications of Genome-Scale Metabolic Models in Biotechnology and Systems Medicine. *Frontiers in Physiology*, *6*. https://doi.org/10.3389/fphys.2015.00413

Figures

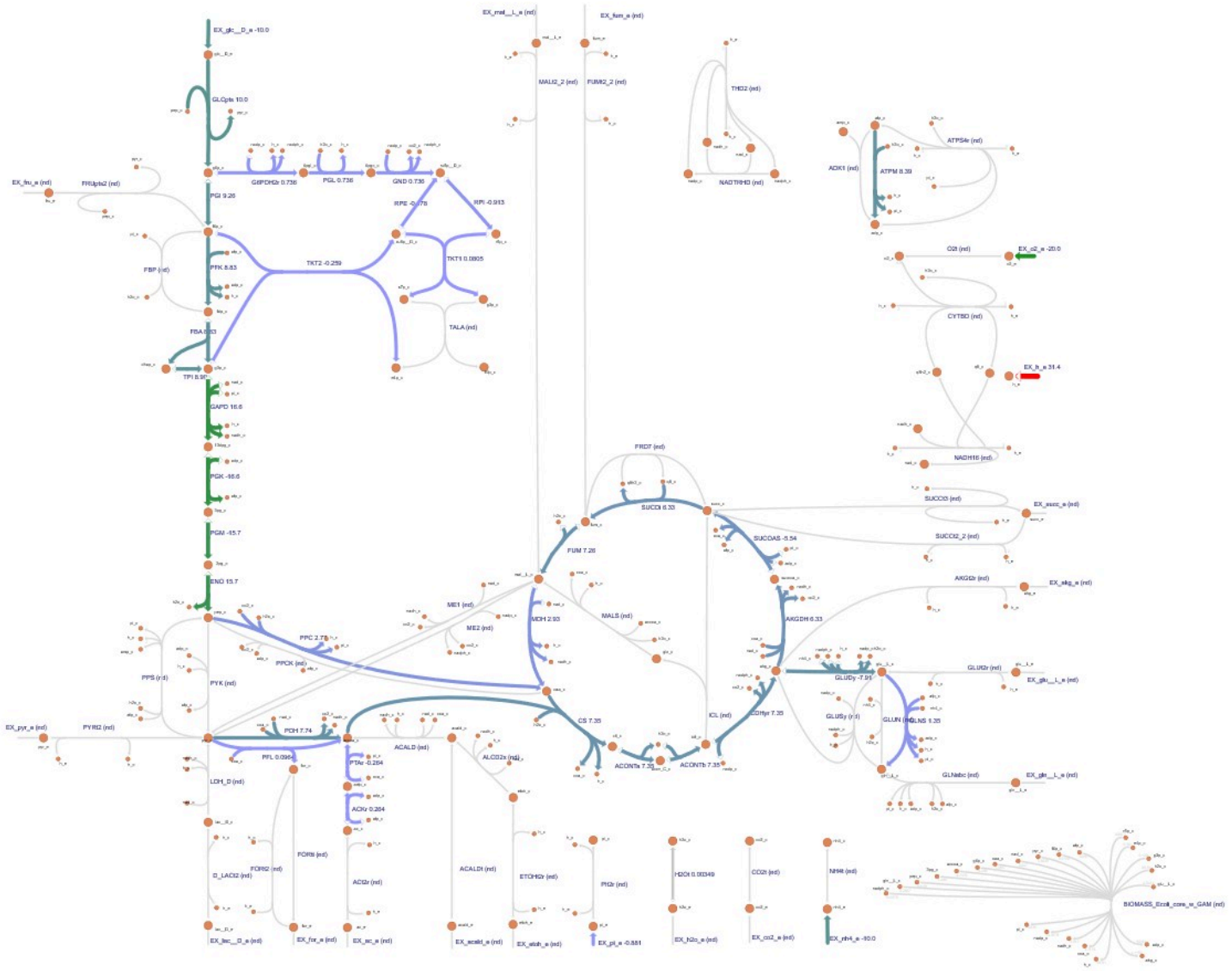


Figure 1

Central carbon metabolic flux distribution in Cronobacter sakazakii ATCC BAA-894 predicted by flux balance analysis under aerobic glucose minimal medium conditions. Carbon fluxes were calculated using the curated genome-scale metabolic model iMN1443 and are presented as mmol gDW^{-1} h^{-1}. Arrow coloration is proportional to the magnitude of the predicted flux. Glucose was assimilated through glycolysis and directed toward pyruvate, which served as a major metabolic branch point. Acetyl-CoA formation occurred predominantly via pyruvate dehydrogenase (PDH) whereas pyruvate formate lyase (PFL) and pyruvate flavodoxin oxidoreductase (PFOR) carried only minor fluxes under the simulated conditions. The majority of acetyl-CoA entered the tricarboxylic acid (TCA) cycle through citrate synthase, supporting active respiratory metabolism. Oxidative phosphorylation was characterized by high flux through NADH dehydrogenase (NADH16pp), cytochrome bo_3 oxidase (CYTBO3_4pp), and ATP synthase (ATPS4rpp), supporting substantial ATP generation. The alternative cytochrome bd oxidase

carried no detectable flux under the simulated conditions, while acetate and formate secretion were not predicted.

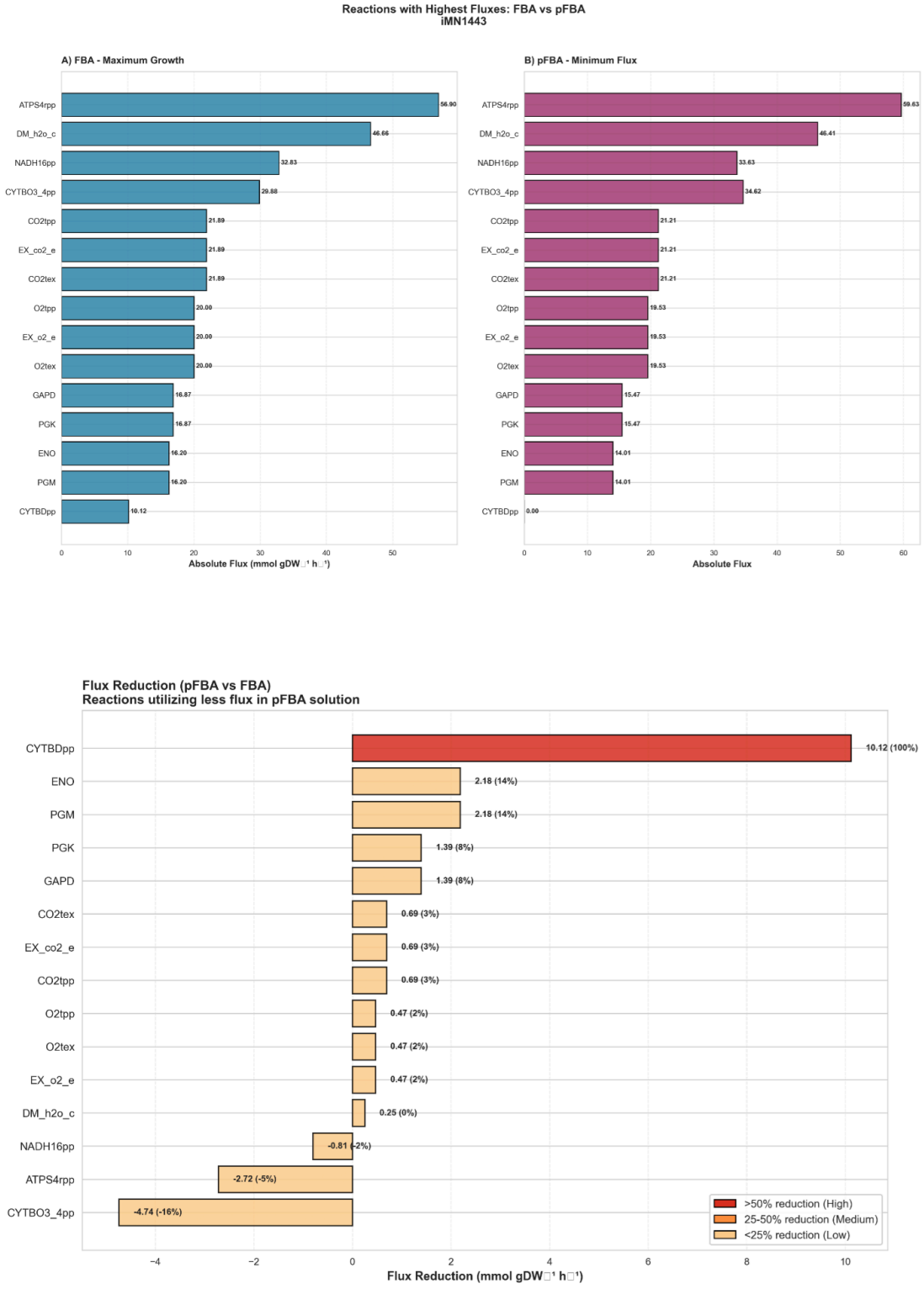


Figure 2

Comparative Flux Balance Analysis (FBA) and Parsimonious Flux Balance Analysis (pFBA) of *Cronobacter sakazakii*(iMN1443). (A) Top: Side-by-side comparison of reactions with the highest

absolute fluxes. The blue bars represent standard FBA while the maroon bars represent pFBA. (B) Bottom: Reactions that exhibit lower flux in the pFBA solution compared to standard FBA. The reduction is categorized by magnitude (High: >50% reduction; Medium: 25–50%; Low: <25%).

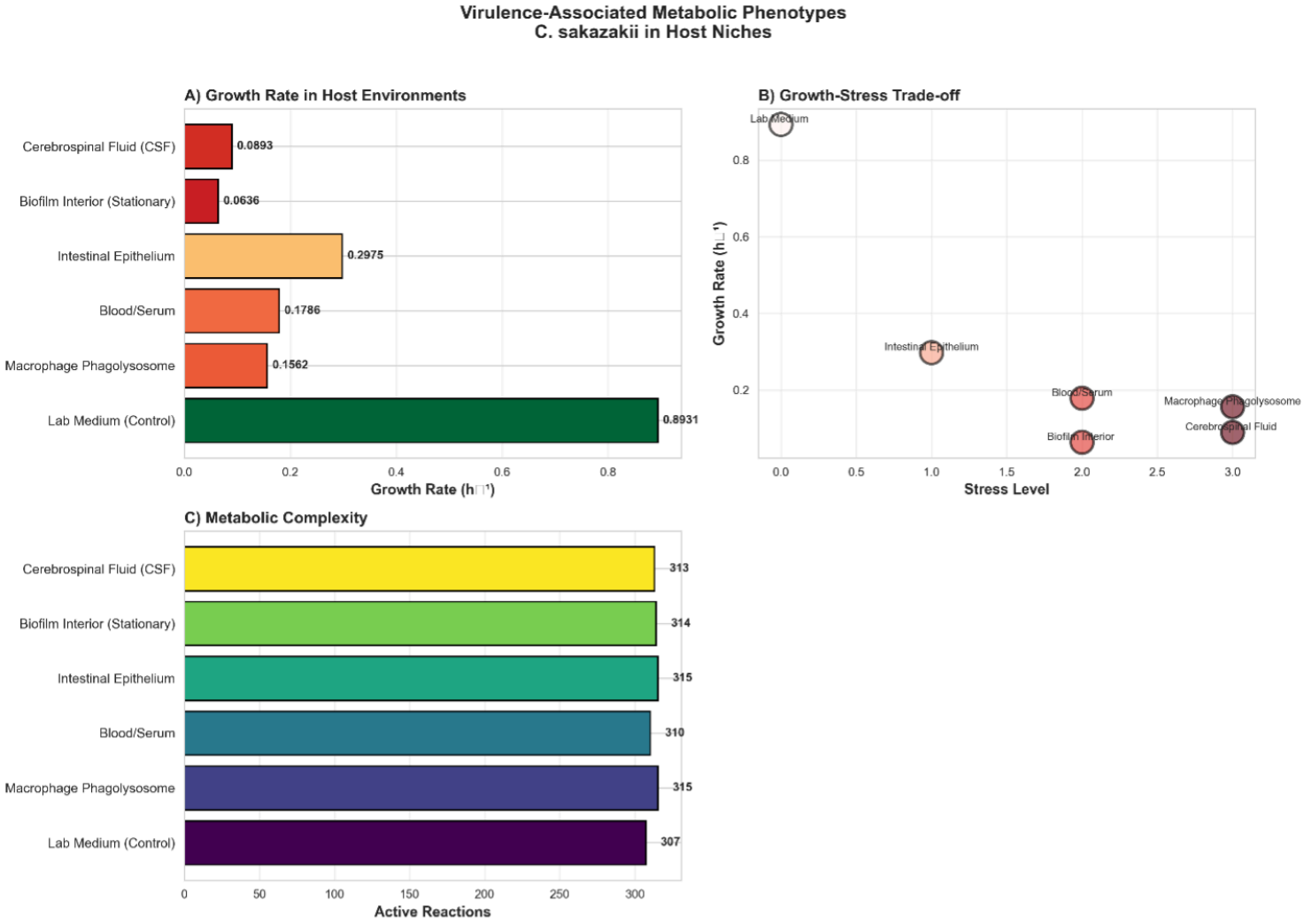


Figure 3

Environment-dependent metabolic phenotypes of *C. sakazakii*. (A) Growth rates across six simulated host niches show inverse relationship with environmental stress. (B) Growth-stress trade-off showing the relationship between stress level and rate of growth in different environments. C) The number active reactions in different environments as a predictor of metabolic complexity.

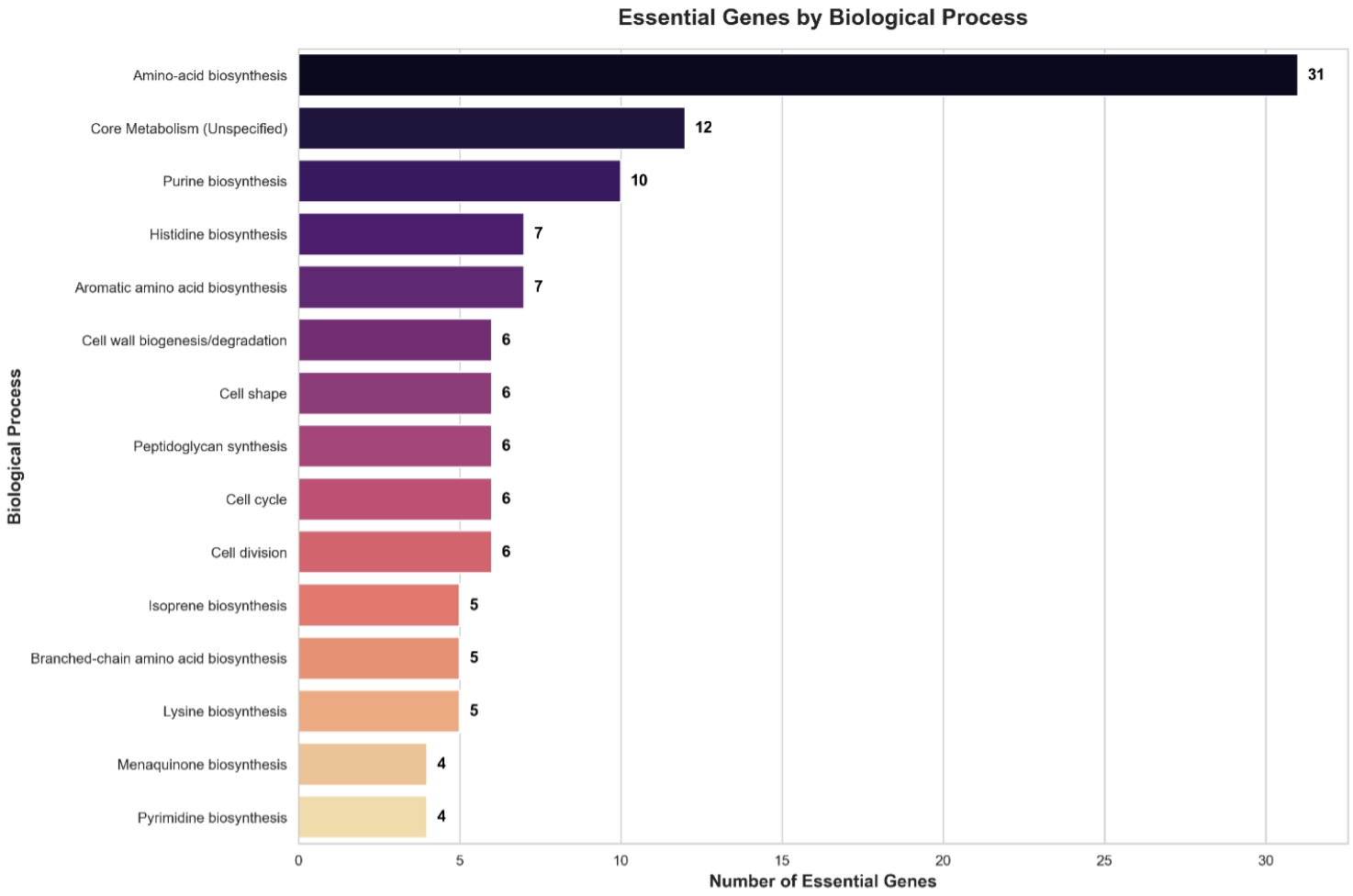


Figure 4

Distribution of predicted essential genes across major biological processes in the iMN1443 model of *Cronobacter sakazakii*. Amino acid biosynthesis represented the largest category, followed by core metabolism and purine biosynthesis. Genes involved in cell wall biogenesis, peptidoglycan synthesis, cell division, and cell cycle regulation also constituted substantial fractions of the essential gene set.

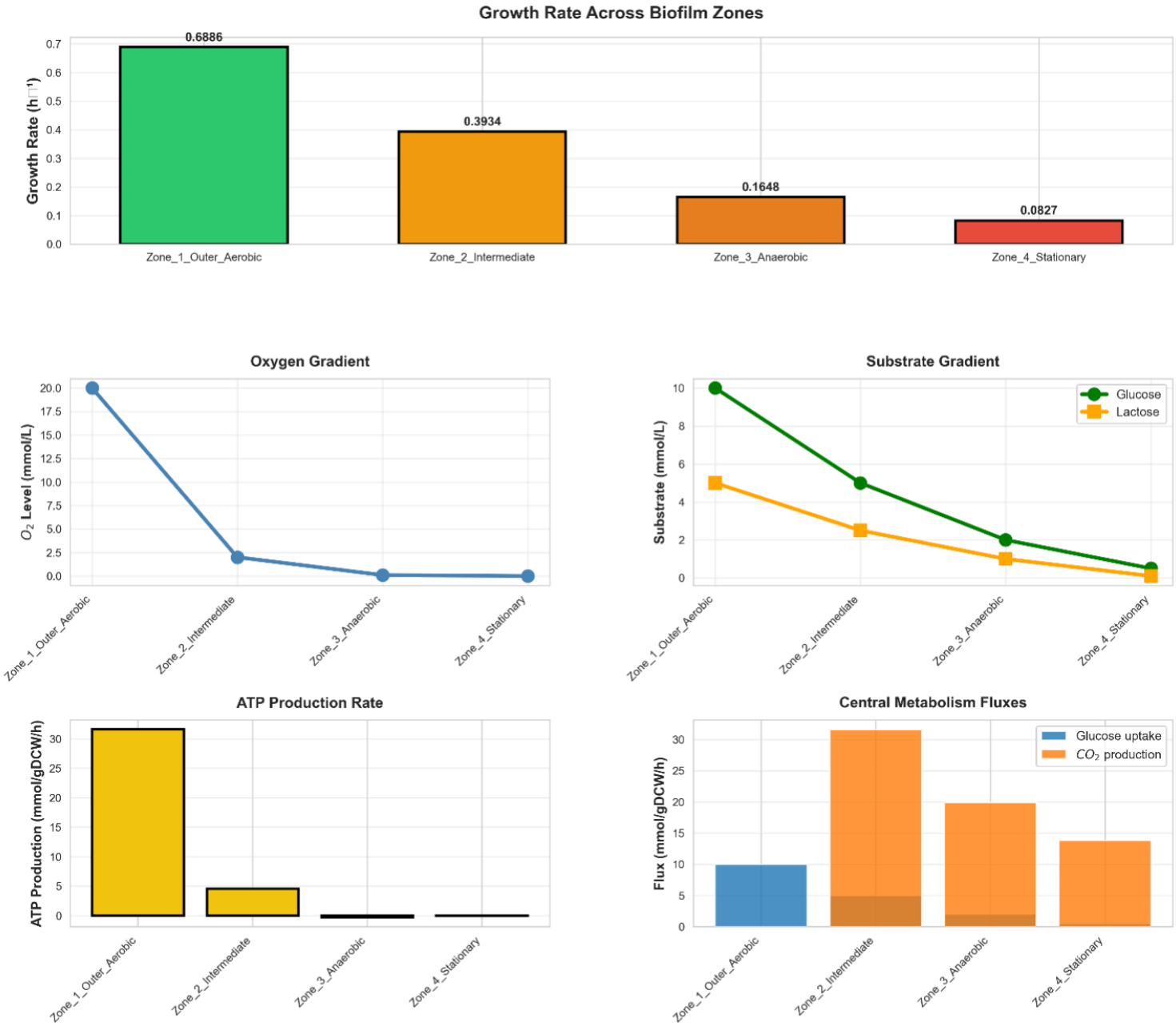


Figure 5

Predicted metabolic stratification of *Cronobacter sakazakii*biofilms using the iMN1443 genome-scale metabolic model. Growth rate, oxygen availability, substrate concentrations, ATP production, and central metabolic fluxes are shown across four simulated biofilm zones representing aerobic surface layers, intermediate microaerophilic regions, anaerobic cores, and nutrient-depleted stationary regions.

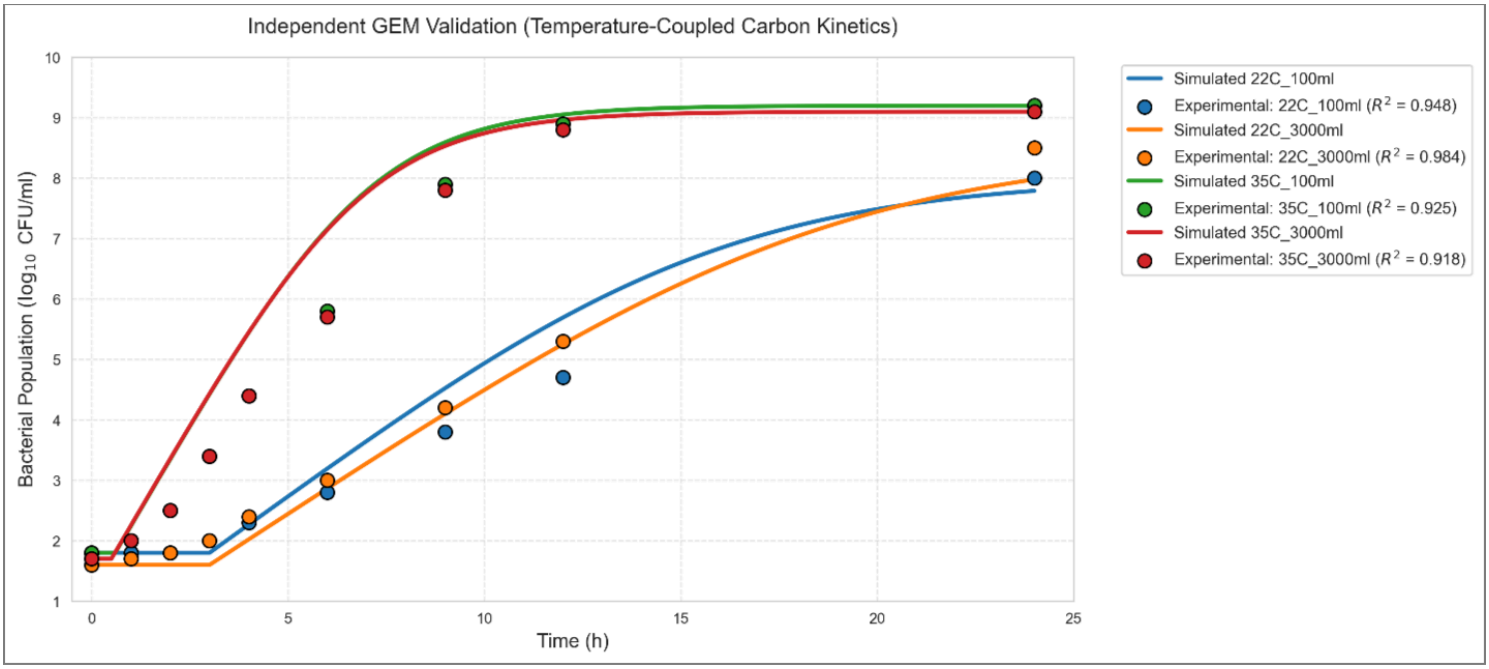


Figure 6

Independent dFBA model validation against empirical growth curves. Simulated growth kinetics (solid lines) compared to experimental observations (dots) at 22°C and 35°C in 100 mL and 3000 mL culture volumes. Carbon uptake bounds were adjusted via Ratkowsky temperature scaling. Goodness-of-fit metrics (R^2 > 0.918 across all conditions) demonstrate high predictive accuracy for temperature-dependent growth rates.